Performance evaluation of analog signal transmission in an integrated optical vortex emitter to 3.6-km few-mode fiber system

JUN LIU,[1,+] SHIMAO LI,[2,+] JING DU,[1,+] CHARALAMBOS KLITIS,[3] CHENG DU,[4] QI MO,[4] MARC SOREL,[3] SIYUAN YU,[2] XINLUN CAI,[2,*] JIAN WANG[1,*]

[1] *Wuhan National Laboratory for Optoelectronics, School of Optical and Electronic Information, Huazhong University of Science and Technology, Wuhan 430074, Hubei, China.*

[2] *State Key Laboratory of Optoelectronic Materials and Technologies and School of Physics and Engineering, Sun Yatsen University, Guangzhou 510275, China.*

[3] *School of Engineering, University of Glasgow, Rankine Building, Oakfield Avenue, Glasgow G12 8LT, UK.*

[4] *Fiberhome Telecommunication Technologies Co. Ltd, Wuhan 430074, China.*

+These authors contributed equally to this work.

**Corresponding author: caixlun5@mail.sysu.edu.cn, jwang@hust.edu.cn*

We experimentally demonstrate and evaluate the performance of an analog signal transmission system with photonic integrated optical vortex emitter and 3.6-km few-mode fiber (FMF) link using orbital angular momentum (OAM) modes. The fabricated photonic integrated device is capable of emitting vector optical vortices carrying well-defined and quantized OAM modes with topological charge *l*=-2 and 2. After propagating through 3.6-km FMF, we measure and assess the spurious free dynamic range (SFDR) of the second-order harmonic distortion (SHD). Moreover, we study the impact of nonlinearity-induced resonance wavelength shift of the optical vortex emitter on the analog link performance as increasing the input optical power. © 2015 Optical Society of America

OCIS codes: *(050.4865) Optical vortices; (070.1170) Analog optical signal processing, (130.3120) Integrated optics devices.*

A light beam carrying orbital angular momentum (OAM) is characterized by a helical-phase front of $\exp(il\theta)$, in which l is the topological charge number, and θ refers to the azimuthal angle. Because of the helical phase structure, the OAM carrying beam twists and features a doughnut intensity profile due to the phase singularity at the beam center [1]. OAM beam is also known as a kind of vortex beam. In 1992, Allen et al. indicated that OAM beam had discrete values of $l\hbar$ per photon along the propagation direction, where $\hbar$ is the reduced Planck constant [2]. Since then, OAM beam has been widely used to explore a variety of novel natural phenomena such as particle trapping, imaging, quantum information processing, and so on [3-6]. Very recently, the distinct features of unlimited charge values of OAM in principle and intrinsic orthogonality among different OAM states facilitate an alternative multiplexing technique i.e. OAM-division multiplexing (ODM). Similar to mode-division multiplexing, ODM actually chooses another OAM mode basis for multiplexing. Lots of research efforts have been devoted to both free-space and fiber-based optical communication systems by employing OAM multiplexing to increase the transmission capacity and spectral efficiency [7-15].

However, in most of previous works, complex and bulky optical OAM emitters are used, which are slow to respond and also cumbersome. This severely limits the prospect of its wide use in future practical systems. In this scenario, a laudable goal would be to develop a micrometer-sized OAM emitter [16]. Meanwhile, the signals carried by OAM modes are digital signals such as m-ary phase-shift keying (m-PSK) and m-ary quadrature amplitude modulation (m-QAM) in most of the OAM transmission experiments [17, 18]. Actually, analog signal transmissions have been also developed in miscellaneous applications, for instance, broadband wireless access networks, sensor networks, radar systems, remote or phased array antennas, and radio-over-optical transmission systems [18-21]. Recently, analog signal transmission in a free-space OAM multiplexing system by two spatial light modulators (SLMs) has been reported [22]. Considering the recent advances of integrated OAM emitter and fiber-based digital signal transmissions using OAM modes to explore the space dimension of a light beam, it would be also interesting to study the impact of OAM beams on analog signal transmissions in an integrated OAM emitter to an OAM fiber link.

In this Letter, we experimentally demonstrate and evaluate the performance of analog signal transmission system with photonic integrated optical vortex emitter and 3.6-km few-mode fiber (FMF) link using OAM modes. The photonic integrated device emits vector optical vortices carrying well-defined and quantized OAM. We generate two OAM modes with topological charge $l = -2$ and 2 carrying analog signal and propagate through a 3.6-km FMF. We analyze the spurious free dynamic range (SFDR) of the second-order harmonic distortion (SHD), which is an important factor used to estimate the analog link performance.

The experimental setup of an analog signal transmission system with photonic integrated optical vortex emitter and 3.6-km FMF link is shown in Fig. 1. At the transmitter side, the output of a tunable laser is injected to an intensity modulator (IM). The light source is modulated by a 3-GHz radio frequency (RF) in the IM, and then amplified by an erbium-doped fiber amplifier (EDFA). A polarization controller (PC) is

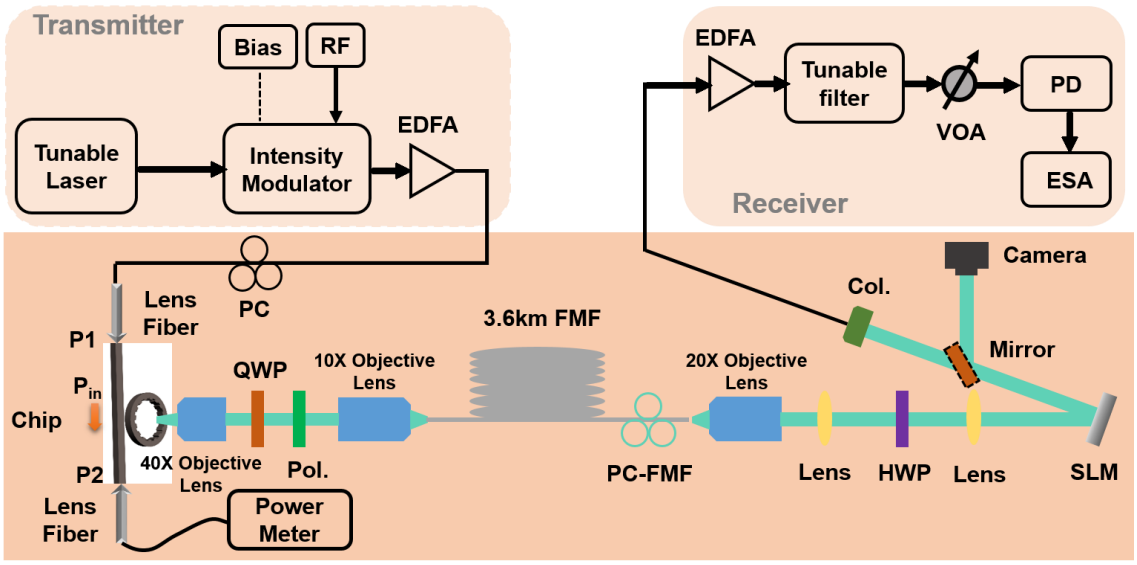

Fig. 1. Experimental setup of an analog signal transmission system with photonic integrated optical vortex emitter and 3.6-km FMF link. RF: radio frequency; PC: polarization controller; EDFA: erbium-doped fiber amplifier; QWP: quarter-wave plate; Pol.: polarizer; FMF: few-mode fiber; PC-FMF: polarization controller on few-mode fiber; HWP: half-wave plate; SLM: spatial light modulator; Col.: collimator; VOA: variable optical attenuator; PD: photodetector; ESA: electric spectrum analyzer.

used to launch light in the quasi-TE mode before the signal is coupled into the input waveguide of the micro-ring resonator, and the power is monitored by a power meter placed at the output port of the waveguide. For the state of polarization (SOP) of the source whispery gallery modes (WGMs) and the angular grating structure are both cylindrically symmetric, the radiated beams should maintain this symmetry and should be cylindrical vector (CV) beams of which the Jones vector E_{CV} can be written as $E_{CV} = \begin{pmatrix} -\sin\theta \\ \cos\theta \end{pmatrix} \exp(il\theta)$. Thus, it can be described as the superposition of two orthogonal scalar vortices, as E_{CV} can be further decomposed into $E_{CV} = \frac{i}{2}\begin{pmatrix} 1 \\ -i \end{pmatrix} \exp i[(l+1)\theta] - \frac{i}{2}\begin{pmatrix} 1 \\ i \end{pmatrix} \exp i[(l-1)\theta]$, which consists of a right-hand circularly polarized (RHCP) beam with topological charge of $l+1$ and a left-hand circularly polarized (LHCP) beam with $l-1$ [16]. After passing through the quarter-wave plate (QWP), the LHCP beam and RHCP beam are converted to two orthogonal linearly polarization beams. Then the linearly polarized OAM beam we need is picked out by a polarizer. In the experiment, we choose OAM_2 at a wavelength of 1531.91 nm and OAM_{-2} at a wavelength of 1556.56 nm. The picked out OAM beams are coupled into the FMF by a 10X objective lens and then propagate through the 3.6-km FMF. polarization controller (PC) placed at the output of the FMF (PC-FMF) is adjusted to obtain the OAM states with the lowest cross-talk. The OAM beam is collimated by a 20X objective lens after propagating through the fiber and then demodulated by the SLM loaded with a reverse phase pattern. The half-wave plate (HWP) is used to adjust the polarization of the output light of FMF aligned to the polarization of the SLM. Finally, the demodulated Gaussian-like beam is coupled into a single-mode fiber (SMF) for detection. At the receiver side, after being amplified by EDFA and attenuated by variable optical attenuator (VOA), the signal is sent to a photo-detector (PD) and then measured by an electric spectrum analyzer (ESA).

We first measure the intensity profiles of the emitted vector vortex modes. Figure 2(a) and (c) show the intensity profiles of OAM_2 at a wavelength of 1531.91 nm and OAM_{-2} at a wavelength of 1556.56 nm after decomposition by the QWP and polarizer, respectively. The interference patterns (i.e. interferograms) of these two modes with a reference Gaussian beam are depicted in Fig. 2(b) and (d) correspondingly. The polarization of the reference Gaussian beam is -45° and 45° with respect to the fast axis of QWP.

We also measure the intensity profiles of the two modes after propagating through the 3.6-km FMF. The intensity profiles of OAM_2 at a wavelength of 1531.91 nm and OAM_{-2} at a wavelength of 1556.56 nm after propagating through 3.6-km FMF are shown in Fig. 3(a) and (c), respectively. Figure 3(b) and (d) show the intensity profiles of the demodulation of these two OAM modes after modulated by the SLM loaded with a reverse phase pattern.

We then evaluate the performance of analog signal transmission in an optical vortex emitter to 3.6-km FMF link using OAM modes. Figure 4(a) and (b) show measured RF spectra before the integrated optical vortex emitter to FMF link by ESA at wavelength of 1531.91 nm and 1556.56 nm, respectively. The resolution bandwidth of the measured RF spectra is 1 kHz.

To further characterize the performance of analog signal transmission in an optical vortex emitter to 3.6-km FMF link, we measure the output power of the RF carrier and distortions as a function of the RF input power of OAM_2 at a wavelength of 1531.91 nm and OAM_{-2} at a wavelength of 1556.56 nm as shown in Fig. 5(a) and (b) respectively. The input power of the optical signal is about 15 dBm. We can see that the analog transmission penalty is induced after transmission through the combined optical vortex emitter and 3.6-km FMF link. SFDR is an important common judgment criterion to measure the linearity of an analog link [23, 24]. SFDR is defined by the RF input power range at the left and right boundaries of which the fundamental RF power and SHD power are equal to the noise floor [25, 26]. In general, a higher SFDR system facilitates a more linear analog signal transmission. SFDRs can be gained by measuring the intercepting points of output power curves (RF carrier, SHD) and the noise floor. As shown in Fig. 5(a), for OAM_2 at a wavelength of 1531.91 nm, the measured SHD SFDRs before the integrated optical vortex emitter to FMF link, after the integrated optical vortex emitter, and after the integrated optical vortex emitter to FMF link are 63.57 dB, 57.97 dB, and 53.25 dB, respectively. As depicted in Fig. 5(b), for OAM_{-2} at a wavelength of 1556.56 nm, the corresponding SHD SFDRs are measured to be 62.3 dB, 57.6 dB, and 52.5 dB, respectively. A 10-dB degradation of SHD SFDR is observed for both two modes after

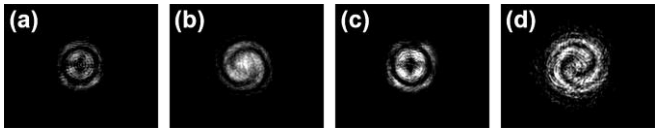

Fig. 2. (a) Measured intensity profile of OAM_2 at a wavelength of 1531.91 nm after decomposition. (b) Measured interference pattern of OAM_2 at a wavelength of 1531.91 nm with a reference Gaussian beam. (c) Measured intensity profile of OAM_{-2} at a wavelength of 1556.56 nm after decomposition. (d) Measured interference pattern of OAM_{-2} at a wavelength of 1556.56 nm with a reference Gaussian beam.

transmission in optical vortex emitter to 3.6-km FMF link. The notable reduction of SHD SFDR is induced by two parts. First, the optical transmission loss plays an important role. The transmission loss is mainly induced by the emission loss of optical vortex emitter, coupling loss from free-space to FMF, coupling loss from free-space to SMF and optical components such as objective lens, SLM, and so on. Second, the SHD SFDR degrades due to the notch filtering effect of the vortex emitter. The sideband caused by RF carrier falls into the 3-dB bandwidth region of the vortex emitter, especially near the notch resonance wavelength. In this case, the vortex emitter actually functions as a filter to eliminate the output fundamental frequency sideband (output RF carrier), while the high-order harmonic sidebands (SHD) survive. In addition, compared to other works, the measured SHD SFDR of back to back system is relatively low [22]. Such phenomenon might be ascribed to the nonlinear response of the modulator and the high-level noise floor of adopted RF source.

In order to fully investigate the analog signal transmission in the 3-dB bandwidth region near the resonance wavelength, we change the input optical power from 15.5 to 18.5 dBm. Figure 6(a) and (b) plot the measured SHD SFDR after transmission of OAM_2 at a wavelength of 1531.91 nm and OAM_{-2} at a wavelength of 1556.56 nm, respectively. One can see that the SHD SFDR varies slightly as changing the input optical power of OAM_2 at a wavelength of 1531.91 nm as shown in Fig. 6(a) and OAM_{-2} at a wavelength of 1556.56 nm as shown in Fig. 6(b). Generally, the SHD SFDR should increase with the input optical power. To explain such interesting phenomena, we measure the radiation and transmission spectra of the vortex emitter when the input optical power is 15, 16, 17 and 18 dBm respectively as shown in Fig. 7(a)-(d) by scanning input laser wavelength. The red points represent the input wavelength of 1531.91 nm and 1556.56 nm. One can see that the resonance wavelength moves towards to longer wavelength as increasing the input optical power. So the actually radiated optical power from the optical vortex emitter for analog signal transmission could change slightly as increasing the input optical power, resulting in slight variation of SHD SFDR as shown in Fig. 6.

In conclusion, we experimentally demonstrate and evaluate the performance of an analog signal transmission system in a photonic integrated optical vortex emitter to 3.6-km FMF link using OAM modes. Two OAM modes generated by the photonic integrated optical vortex emitter propagate through the FMF link. SHD SFDR is used to assess the

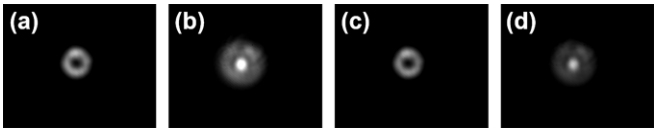

Fig. 3. Measured intensity profiles of (a) OAM_2 at a wavelength of 1531.91 nm after propagating through 3.6-km FMF, (b) demodulation of OAM_2 at a wavelength of 1531.91 nm after SLM, (c) OAM_{-2} at a wavelength of 1556.56 nm after propagating through 3.6-km FMF, (d) demodulation of OAM_{-2} at a wavelength of 1556.56 nm after SLM.

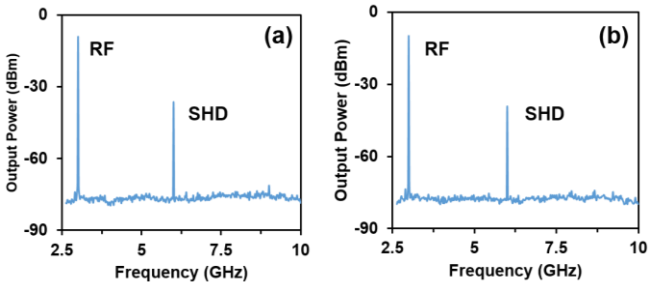

Fig. 4. (a) Measured RF spectra of RF carrier and SHD by ESA at a wavelength of 1531.91 nm before the vortex emitter to FMF link. (b) Measured RF spectra of RF carrier and SHD by ESA at a wavelength of 1556.56 nm before the vortex emitter to FMF link.

analog link performance. The influences of input optical power on the analog signal transmission are studied. For relatively high input optical power, the analog signal transmission might be also affected by the nonlinearity-induced resonance wavelength shift of the photonic integrated optical vortex emitter.

Funding. The National Basic Research Program of China (973 Program, 2014CB340004); National Natural Science Foundation of China (NSFC) (11274131, 11574001, 61222502); Program for New Century

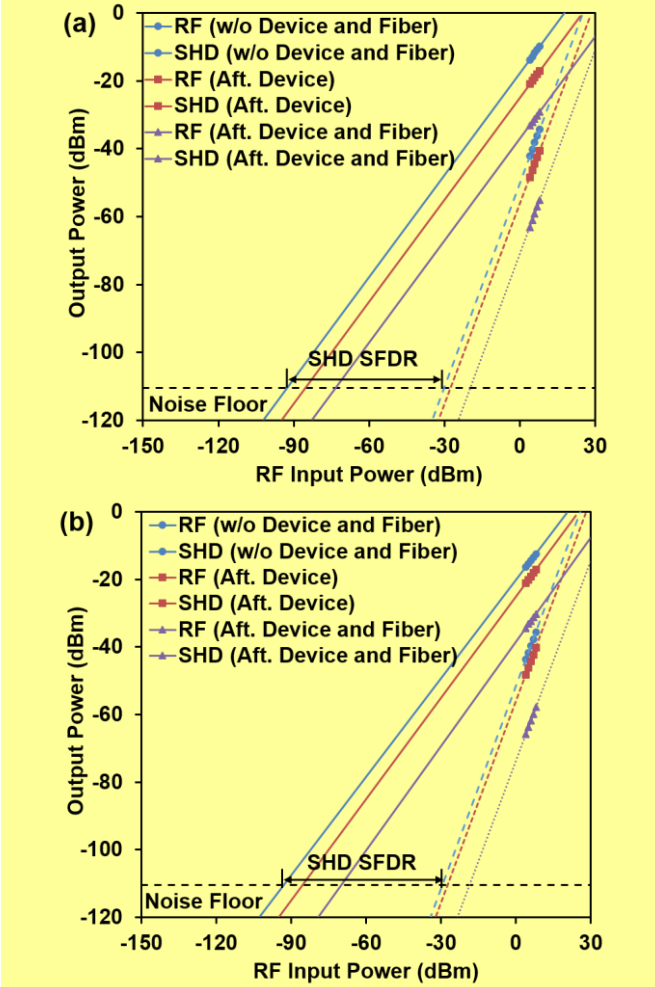

Fig. 5. Measured output power of RF carrier and distortions versus RF input power of (a) OAM_2 at a wavelength of 1531.91 nm and (b) OAM_{-2} at a wavelength of 1556.56 nm.

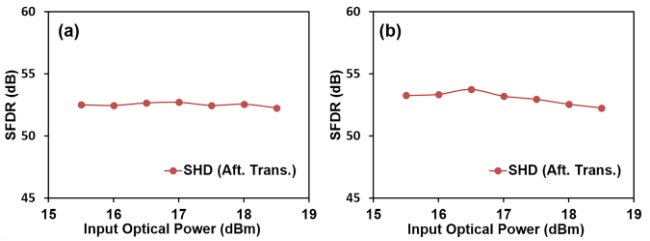

Fig. 6. Measured SHD SFDR after transmission versus input optical power of (a) OAM_2 at a wavelength of 1531.91 nm and (b) OAM_{-2} at a wavelength of 1556.56 nm.

Excellent Talents in University (NCET-11-0182); Wuhan Science and Technology Plan Project (2014070404010201); seed project of Wuhan National Laboratory for Optoelectronics (WNLO).

Acknowledgment. We thank the staff of the James Watt Nanofabrication Centre at Glasgow University for technical support.

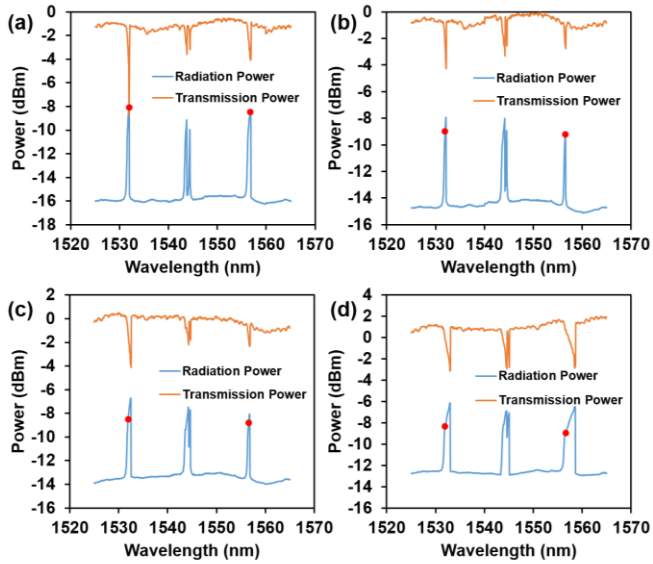

Fig. 7. Measured radiation and transmission spectra of the vortex emitter with a radius of 14 μm when the input optical power is (a) 15 dBm, (b) 16 dBm, (c) 17 dBm, and (d) 18 dBm, respectively.

References

1. A. M. Yao and M. J. Padgett, Adv. Opt. Photon. **3**, 161 (2011).
2. L. Allen, M. W. Beijersbergen, R. Spreeuw, and J. P. Woerdman, Phys. Rev. A **45**, 8185 (1992).
3. D. Grier, Nature **424**, 810 (2003).
4. M. Padgett, R. Bowman, Nat. Photonics **5**, 343 (2011).
5. S. Fürhapter, A. Jesacher, S. Bernet, and M. Ritsch-Marte, Opt. Express **13**, 689 (2005).
6. A. Mair, A. Vaziri, G. Weihs, and A. Zeilinger, Nature **412**, 313 (2001).
7. J. Wang, J.-Y. Yang, I. M. Fazal, N. Ahmed, Y. Yan, H. Huang, Y. Ren, Y. Yue, S. Dolinar, and M. Tur, Nat. Photonics **6**, 488 (2012).
8. A. E. Willner, J. Wang, and H. Huang, Science **337**, 655 (2012).
9. N. Bozinovic, Y. Yue, Y. Ren, M. Tur, P. Kristensen, H. Huang, A. E. Willner, and S. Ramachandran, Science **340**, 1545 (2013).
10. A. Willner, H. Huang, Y. Yan, Y. Ren, N. Ahmed, G. Xie, C. Bao, L. Li, Y. Cao, and Z. Zhao, Adv. Opt. Photon. **7**, 66 (2015).
11. J. Wang, S. Li, C. Li, L. Zhu, C. Gui, D. Xie, Y. Qiu, Q. Yang, and S. Yu, in Optical Fiber Communication Conference (OFC2014), paper W1H. 4. (2014).
12. H. Huang, G. Xie, Y. Yan, N. Ahmed, Y. Ren, Y. Yue, D. Rogawski, M. J. Willner, B. I. Erkmen, and K. M. Birnbaum, Opt. Lett. **39**, 197 (2014).
13. J. Wang, S. Li, M. Luo, J. Liu, L. Zhu, C. Li, D. Xie, Q. Yang, S. Yu, and J. Sun, in European Conference and Exhibition on Optical Communication (ECOC2014), paper Mo.4.5.1 (2014).
14. A. Wang, L. Zhu, J. Liu, C. Du, Q. Mo, and J. Wang, Opt. Express **23**, 29457 (2015).
15. J. Wang, J. Liu, X. Lv, L. Zhu, D. Wang, S. Li, A. Wang, Y. Zhao, Y. Long, J. Du, X. Hu, N. Zhou, S. Chen, L. Fang, and F. Zhang, in European Conference and Exhibition on Optical Communication (ECOC2015), paper Th.2.5.4 (2015).
16. X. Cai, J. Wang, M. J. Strain, B. Johnson-Morris, J. Zhu, M. Sorel, J. L. O'Brien, M. G. Thompson, and S. Yu, Science **338**, 363 (2012).
17. P. J. Winzer, IEEE Leos Newsletter **23**, 4 (2009).
18. J. D. Downie, J. Hurley, J. Cartledge, S. Bickham, and S. Mishra, Opt. Express **19**, B96 (2011).
19. J. P. Yao, J. Lightwave Technol. **27**, 314 (2009).
20. H. Kosek, Y. He, X. Gu, and X. N. Fernando, J. Lightwave Technol. **25**, 1401 (2007).
21. J. Du and J. Wang, Opt. Lett. **40**, 1181 (2015).
22. S. Li and J. Wang, Opt. Lett. **40**, 760 (2015).
23. C. H. Cox, *Analog optical links: theory and practice* (Cambridge University Press, 2006).
24. W. S. Chang, *RF photonic technology in optical fiber links* (Cambridge University Press, 2002).
25. W. B. Bridges and J. H. Schaffner, IEEE Trans. Microwave Theor. Tech. **43**, 2184 (1995).
26. C. H. Cox III, E. Ackerman, G. E. Betts, and J. L. Prince, IEEE Trans. Microwave Theory Tech. **54**, 906 (2006).

Full References

1. A. M. Yao and M. J. Padgett, "Orbital angular momentum: origins, behavior and applications," Adv. Opt. Photon. **3**, 161-204 (2011).
2. L. Allen, M. W. Beijersbergen, R. Spreeuw, and J. Woerdman, "Orbital angular momentum of light and the transformation of Laguerre-Gaussian laser modes," Phys. Rev. A **45**, 8185 (1992).
3. D. G. Grier, "A revolution in optical manipulation," Nature **424**, 810-816 (2003).
4. M. Padgett and R. Bowman, "Tweezers with a twist," Nat. Photonics **5**, 343-348 (2011).
5. S. Fürhapter, A. Jesacher, S. Bernet, and M. Ritsch-Marte, "Spiral phase contrast imaging in microscopy," Opt. Express **13**, 689-694 (2005).
6. A. Mair, A. Vaziri, G. Weihs, and A. Zeilinger, "Entanglement of the orbital angular momentum states of photons," Nature **412**, 313-316 (2001).
7. J. Wang, J.-Y. Yang, I. M. Fazal, N. Ahmed, Y. Yan, H. Huang, Y. Ren, Y. Yue, S. Dolinar, and M. Tur, "Terabit free-space data transmission employing orbital angular momentum multiplexing," Nat. Photonics **6**, 488-496 (2012).
8. A. E. Willner, J. Wang, and H. Huang, "A different angle on light communications," Science **337**, 655-656 (2012).
9. N. Bozinovic, Y. Yue, Y. Ren, M. Tur, P. Kristensen, H. Huang, A. E. Willner, and S. Ramachandran, "Terabit-scale orbital angular momentum mode division multiplexing in fibers," Science **340**, 1545-1548 (2013).
10. A. Willner, H. Huang, Y. Yan, Y. Ren, N. Ahmed, G. Xie, C. Bao, L. Li, Y. Cao, and Z. Zhao, "Optical communications using orbital angular momentum beams," Adv. Opt. Photon. **7**, 66-106 (2015).
11. J. Wang, S. Li, C. Li, L. Zhu, C. Gui, D. Xie, Y. Qiu, Q. Yang, and S. Yu, "Ultra-high 230-bit/s/Hz spectral efficiency using OFDM/OQAM 64-QAM signals over pol-muxed 22 orbital angular momentum (OAM) modes," in Optical Fiber Communication Conference (OFC2014), paper W1H. 4. (2014).
12. H. Huang, G. Xie, Y. Yan, N. Ahmed, Y. Ren, Y. Yue, D. Rogawski, M. J. Willner, B. I. Erkmen, and K. M. Birnbaum, "100 Tbit/s free-space data link enabled by three-dimensional multiplexing of orbital angular momentum, polarization, and wavelength," Opt. Lett. **39**, 197-200 (2014).
13. J. Wang, S. Li, M. Luo, J. Liu, L. Zhu, C. Li, D. Xie, Q. Yang, S. Yu, and J. Sun, "N-Dimentional multiplexing link with 1.036-Pbit/s transmission capacity and 112.6-bit/s/Hz spectral efficiency using OFDM-8QAM signals over 368 WDM pol-muxed 26 OAM modes," in European Conference and Exhibition on Optical Communication (ECOC2014), paper Mo.4.5.1 (2014).

14. A. Wang, L. Zhu, J. Liu, C. Du, Q. Mo, and J. Wang, "Demonstration of hybrid orbital angular momentum multiplexing and time-division multiplexing passive optical network," Opt. Express **23**, 29457-29466 (2015).
15. J. Wang, J. Liu, X. Lv, L. Zhu, D. Wang, S. Li, A. Wang, Y. Zhao, Y. Long, J. Du, X. Hu, N. Zhou, S. Chen, L. Fang, and F. Zhang, "Ultra-high 435-bit/s/Hz spectral efficiency using N-dimentional multiplexing and modulation link with pol-muxed 52 orbital angular momentum (OAM) modes carrying Nyquist 32-QAM signals," in European Conference and Exhibition on Optical Communication (ECOC2015), paper Th.2.5.4 (2015).
16. X. Cai, J. Wang, M. J. Strain, B. Johnson-Morris, J. Zhu, M. Sorel, J. L. O'Brien, M. G. Thompson, and S. Yu, "Integrated compact optical vortex beam emitters," Science **338**, 363-366 (2012).
17. P. J. Winzer, "Modulation and multiplexing in optical communication systems," IEEE Leos Newsletter **23**, 4-10 (2009).
18. J. D. Downie, J. Hurley, J. Cartledge, S. Bickham, and S. Mishra, "112 Gb/s PM-QPSK transmission up to 6000 km with 200 km amplifier spacing and a hybrid fiber span configuration," Opt. Express **19**, B96-B101 (2011).
19. J. Yao, "Microwave photonics," J. Lightwave Technol. **27**, 314-335 (2009).
20. H. Kosek, Y. He, X. Gu, and X. N. Fernando, "All-optical demultiplexing of WLAN and cellular CDMA radio signals," J. Lightwave Technol. **25**, 1401-1409 (2007).
21. J. Du and J. Wang, "Experimental performance evaluation of analog signal transmission in a silicon microring resonator," Opt. Lett. **40**, 1181-1184 (2015).
22. S. Li and J. Wang, "Performance evaluation of analog signal transmission in an orbital angular momentum multiplexing system," Opt. Lett. **40**, 760-763 (2015).
23. C. H. Cox, *Analog optical links: theory and practice* (Cambridge University Press, 2006).
24. W. S. Chang, *RF photonic technology in optical fiber links* (Cambridge University Press, 2002).
25. W. B. Bridges and J. H. Schaffner, "Distortion in linearized electrooptic modulators," IEEE Trans. Microwave Theor. Tech. **43**, 2184-2197 (1995).
26. C. H. Cox III, E. Ackerman, G. E. Betts, and J. L. Prince, "Limits on the performance of RF-over-fiber links and their impact on device design," IEEE Trans. Microwave Theory Tech. **54**, 906-920 (2006).